https://dx.doi.org/10.21577/0103-5053.20220122

J. Braz. Chem. Soc., Vol. 34, No. 3, 441-451, 2023
©2023 Sociedade Brasileira de Química

Article

Evaluation of an Industrial Absorption Process for Carbon Capture Using K_2CO_3 Promoted by Boric Acid

Suênia F. de Vasconcelos,[a] Lucas O. Carneiro,[a] Romildo P. Brito[a] and Karoline D. Brito *,[a]

[a]*Departamento de Engenharia Química, Universidade Federal de Campina Grande, 58109-970 Campina Grande-PB, Brazil*

Hot potassium carbonate (HPC) process aims to remove the CO_2 present on synthesis gas. This removal is done in an absorption process, where takes place the reaction of CO_2 with a K_2CO_3 solution. This reaction is slow and H_3BO_3 can be used to increase the rate of reaction. The rate-based model is the most suitable way to model the process. This approach uses different correlations to calculate important mass transfer and hydraulic parameters, such as: mass transfer coefficient, interfacial area, and liquid holdup. This paper aims to evaluate the performance of many correlations to represent the HPC process. An automatic procedure was developed to test a high number of equations, using MATLAB and Aspen Plus software. The best set of correlations was found after a comparison with industrial data. Correlations with errors less than 10% for the entire evaluated operating conditions were calculated for mass transfer coefficient and the interfacial area, as well as for liquid holdup.

Keywords: carbon capture, rate-based model, potassium carbonate, liquid holdup, mass transfer, interfacial area, synthesis gas

Introduction

The hot potassium carbonate (HPC) process was developed in 1950s by Benson and Field to remove the carbon dioxide (CO_2) present in the synthesis gas. Since then, it is one of the most used processes for carbon capture in the industry, with more than 850 plants in operation around the world.[1]

The solvent used in the HPC process is potassium carbonate (K_2CO_3). The main advantages of using K_2CO_3 are lower energy consumption when compared to other solvents; lower toxicity in comparison with ammonia (NH_3), and amines; lower capital cost, as it does not demand a high level of heat integration and it does not show serious corrosion problems.[2]

The HPC process has two main drawbacks: the K_2CO_3 concentration in the solution is limited due to precipitation of the bicarbonate salts; and the reaction kinetics of K_2CO_3 with CO_2 is quite slow when compared to other solvents. Promoters can be used to improve the reaction kinetics and boric acid (H_3BO_3) has shown excellent results, both on pilot and industrial scales.[1]

To have an accurate representation of the HPC process, the rate-based model must be used. It is based on the Maxwell-Stefan equations[3] and on the Two Films Theory[4] and depends on the choice of mass transfer and hydraulic correlations. They are used to predict mass transfer coefficient, interfacial area, and liquid holdup.

Previous works investigated how those correlations impact the model prediction of a CO_2 capture process. Gaspar and Cormos[5] evaluated different combinations of correlations to estimate the mass transfer coefficient, interfacial area, and liquid holdup for amine-based systems. The results were compared with experimental data from four different pilot plants and validated according to the CO_2 composition profile in the absorption column. The correlation proposed by Wang *et al.*[6] provided the best results for the prediction of the mass transfer coefficient and the interfacial area, while the correlation of Rocha *et al.*[7] showed the best performance for predicting liquid holdup.

Zhang and Chen[8] used the equations proposed by Bravo and co-workers[7] to calculate the mass transfer coefficients and evaluated the performance of these equations based on the results of 19 experiments using monoethanolamine (MEA) as solvent. The validation variables were the loading of the rich solution at the absorber

*e-mail: karoline.dantas@ufcg.edu.br
Editor handled this article: Eduardo Carasek

bottom, the fraction of CO_2 removed, and the energy consumption in the stripper column. The authors obtained errors lower than 7% for all cases.

Qi *et al.*[9] used the equations proposed by Onda *et al.*[10] for the calculation of mass transfer coefficients and interfacial area, and the equation of Stichlmair *et al.*[11] for estimating liquid holdup. The model results were compared with experimental data from a CO_2 absorption column using NH_3 as solvent, and the validation variables were the CO_2 removal rate, NH_3 composition in the clean gas, absorber temperature profile, and the global mass transfer coefficient. The results showed significant errors for the estimation of the CO_2 removal rate and for the NH_3 composition in the clean gas.

Hemmati *et al.*[12] evaluated the combination of several correlations for calculating the mass transfer coefficient, interfacial area, and liquid holdup, to predict the behavior of the CO_2 capture process with a solution of methyldiethanolamine using piperazine as additive. The obtained results were compared to 24 experiments carried out in a pilot plant and indicated that the equation of Bravo and co-workers[7] was the most suitable for the mass transfer coefficient and interfacial area calculations. To calculate the liquid holdup, the equations of Stichlmair *et al.*[11] and Billet and Schultes[13] provided the same results. The validation variables were the absorber temperature profile, rich solution loading, and fraction of CO_2 captured.

Considering the carbon capture using potassium carbonate promoted with H_3BO_3, there is no study in the literature which says what are the suitable mass transfer and hydraulic correlations. This paper presents the Aspen Plus[14] simulation of the HPC process and the assessment of several correlations to calculate mass transfer coefficient, liquid holdup, and interfacial area. The developed model was validated against plant data and the best set of correlations was found. As the assessment of many correlations is an exhaustive process, an automatic procedure was developed to do it.

Experimental

The HPC process investigated in this work is in an ethylene oxide industrial plant and it is highlighted in Figure 1. Carbon dioxide is a by-product of the ethylene oxide reactor, which should be removed to avoid a decrease in catalyst selectivity. The formation of CO_2 in the reactor increases when the lifetime catalyst approaches its end.[15]

After leaving the ethylene oxide recovery column, the CO_2-rich gas (FGAS) exchanges heat with the lean solution (LSOL) and it is fed into the base of the absorption column (ABS), while the solution enters at the top. The contact between the phases occurs through a countercurrent flow inside the column, enabling the absorption and diffusion of CO_2 in the K_2CO_3 solution promoted with H_3BO_3 and the consequent gas purification.

The treated gas leaves the top of the absorption column and is partially condensed to remove water. The vapor

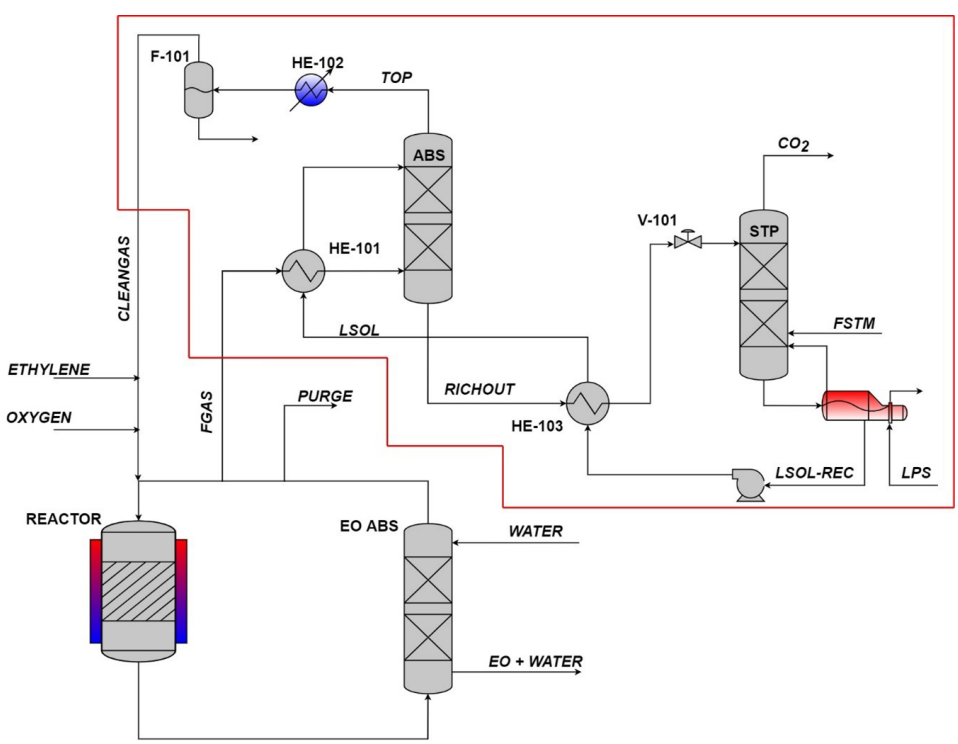

Figure 1. Industrial process flow diagram of the hot potassium carbonate of an ethylene oxide industrial plant.

stream (CLEANGAS) is recycled back to reactor, as shown in Figure 1.

The rich solution of K_2CO_3 that leaves the absorber at the bottom (RICHOUT) exchanges heat with the recirculated lean solution (LSOL-REC) and then enters in the top stage of the stripper column (STP). Low-pressure steam (FSTM) is fed directly into the stripper, promoting the CO_2 desorption, and regenerating the solution's absorption capacity. The removed CO_2 (CO2) is sold to oxygen factories, and the lean solution is pumped back to top stage of the absorption column.

The focus of the paper (the absorption column and the stripper column) is the part highlighted in red, which is shown in Figure 2 (simulated in Aspen Plus). The specifications of each equipment are presented in Table 1.

Figure 2 also presents the average data of the process variables, measured over 20 months of operation. These data are later used to validate the best set of correlations that should be used in the evaluated absorption process.

Modelling

The HPC process promoted with H_3BO_3 has a high number of electrolytes in the liquid phase. The suitable thermodynamic model to describe the behavior of this system is the electrolytic nonrandom two-liquid (ELECNRTL).[2,5] As the absorption column operates at high pressures, the Redlich-Kwong equation of state is used for the vapor phase.

The chemical species defined as Henry components were argon (Ar), carbon dioxide (CO_2), nitrogen (N_2), oxygen (O_2), methane (CH_4), ethylene (C_2H_4), ethylene oxide (C_2H_4O), and ethane (C_2H_6). Under the process conditions, all these components are beyond their critical point, except ethylene oxide (C_2H_4O); however, due to its extremely low composition, the Henry's law can also be applied to this component.

Equation 1 shows the calculation of Henry's law constant ($H_{i,j}$) for a component i dissolved in a solvent j as a function of temperature (T):

$$\ln\left(H_{i,j}\right) = a_{ij} + \frac{b_{ij}}{T} + c_{ij}\ \ln\left(T\right) + d_{ij}T \tag{1}$$

The parameters a_{ij}, b_{ij}, c_{ij}, and d_{ij} for C_2H_4O were obtained from Conway *et al.*,[16] while the parameters of the components were determined through numerical regression from the Aspen Plus databank. Table 2 presents the parameters for the solute and solvent pairs regarding the process under study.

Chemical reactions

The overall reaction of the CO_2 absorption process with a K_2CO_3 solution is described by reaction 2:[17]

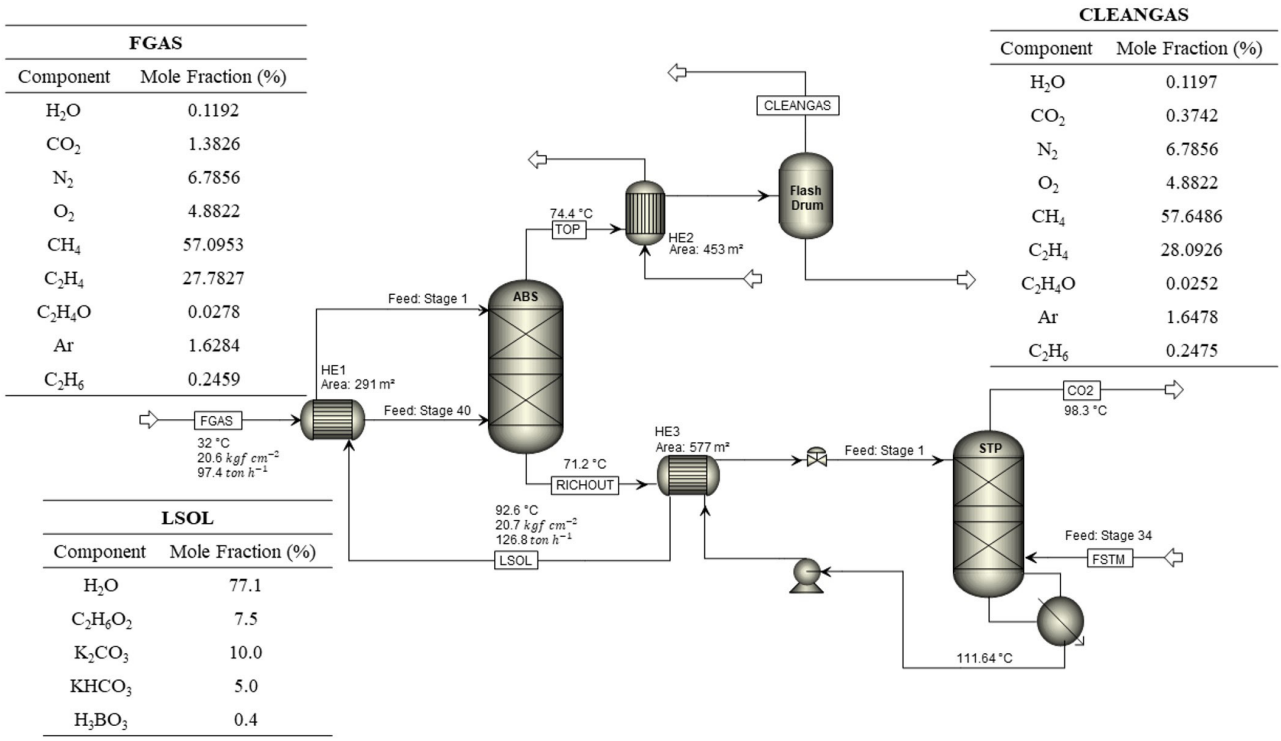

Figure 2. Process flowsheet diagram implemented in Aspen Plus software.

$$CO_2 + K_2CO_3 + H_2O \rightleftharpoons 2KHCO_3 \quad (2)$$

K_2CO_3 and $KHCO_3$ are strong electrolytes, which completely and quickly dissociate in contact with water; therefore, it is possible to consider that they are present in the liquid phase only in the form of K^+ ions, according to the following reactions:[17,18]

$$K_2CO_3 \rightarrow 2K^+ + CO_3^{2-} \quad (3)$$
$$KHCO_3 \rightarrow K^+ + HCO_3^- \quad (4)$$

Therefore, the reaction 2 can be re-written in the form:

$$CO_2 + CO_3^{2-} + H_2O \rightleftharpoons 2HCO_3^- \quad (5)$$

Reaction 5 is not instantaneous; it occurs from a sequence of elementary reactions. There are two reaction mechanisms involved in the overall reaction, which are dependent on the pH of the solution. In alkaline conditions (pH > 8), which is the case of the present process, the reaction mechanism is based on the formation of HCO_3^- (reaction 6) and on the equilibrium reaction between bicarbonate and carbonate (reaction 7).[17]

$$CO_2 + OH^- \rightleftharpoons HCO_3^- \quad (6)$$
$$CO_3^{2-} + H_3O^+ \rightleftharpoons HCO_3^- + H_2O \quad (7)$$

The water dissociation (reaction 8) is also present in this mechanism:

$$2H_2O \rightleftharpoons H_3O^+ + OH^- \quad (8)$$

Reaction 6 was modeled by the forward (9) and reverse (10) reactions:[18,19]

$$CO_2 + OH^- \rightarrow HCO_3^- \quad (9)$$
$$HCO_3^- \rightarrow CO_2 + OH^- \quad (10)$$

It is well known that the explained reaction mechanism is quite slow. Aiming to increase the rate of reaction 7, and, consequently, the CO_2 removal efficiency of the process, a boric acid solution (H_3BO_3) is used, which acts as a catalyst in the process. Boron hydroxide(IV) ($B(OH)_4^-$) reacts with CO_2 to improve the formation of HCO_3^- through the following mechanism:[19]

$$H_3BO_3 + H_2O \rightleftharpoons B(OH)_4^- + H^+ \quad (11)$$
$$B(OH)_4^- + CO_2 \rightarrow B(OH)_4CO_2^- \quad (12)$$
$$B(OH)_4CO_2^- + H_2O \rightarrow H_3BO_3 \cdot H_2O + HCO_3^- \quad (13)$$

Table 1. Absorption and stripper columns specifications

Equipment	Calculation routine	Specification
ABS	RateFrac	pressure: 20.7 kgf cm^{-2} stages number: 40 packing: structured MELLAPAK 250Y packing height: 19.52 m column diameter: 2.38 m
STP	RateFrac	pressure: 1.1 kgf cm^{-2} stages number: 35 packing: random FLEXIMAX 300 packing height: 17.68 m column diameter: 1.68 m steam (FSTM) feed stage: 34

ABS: absorber; STP: stripper; FSTM: low-pressure steam.

Table 2. Henry's law binary parameters

Component i	Component j	a_{ij}	b_{ij}	c_{ij}	d_{ij}	Temperature unit	Pressure unit
CO_2	H_2O	159.2	−8477.7	−21.96	0.0058	°C	bar
N_2	H_2O	164.99	−8432.8	−21.56	−0.0084	°C	bar
O_2	H_2O	144.41	−7775.0	−18.4	−0.0094	°C	bar
CH_4	H_2O	183.78	−9111.7	−25.04	0.00014	°C	bar
C_2H_4	H_2O	152.94	−7959.7	−20.51	0	°C	bar
Ar	H_2O	169.48	−8137.13	−23.25	0.0031	°C	bar
C_2H_6	H_2O	268.43	−13368.1	−37.55	0.0023	°C	bar
C_2H_4O	H_2O	24.5	−3200	0	0	K	Pa
CO_2	$C_2H_6O_2$	−83.82	2941.4	14.05	0	°C	bar
N_2	$C_2H_6O_2$	10.21	0	0	0	°C	bar
O_2	$C_2H_6O_2$	9.89	0	0	0	°C	bar
CH_4	$C_2H_6O_2$	8.68	0	0	0	°C	bar
C_2H_4	$C_2H_6O_2$	−1.99	2751.5	0	0	°C	bar
Ar	$C_2H_6O_2$	8.86	161.1	0	0	°C	bar
C_2H_6	$C_2H_6O_2$	10.24	−822.03	0	0	°C	bar

a_{ij}, b_{ij}, c_{ij}, and d_{ij}: parameters for C_2H_4O were obtained from Conway *et al.*[14]

To model the reaction mechanism of H_3BO_3 in Aspen Plus, reactions 12 and 13 are replaced by a single global reaction, resulting in reaction 14:[18]

$$B(OH)_4^- + CO_2 \rightarrow H_3BO_3 + HCO_3^- \quad (14)$$

The ethylene oxide present in the vapor phase, when diffusing into the liquid phase, reacts with water to form monoethylene glycol ($C_2H_6O_2$), according to:

$$C_2H_4O + H_2O \rightleftharpoons C_2H_6O_2 \quad (15)$$

Only the direct path of reaction 15 is modeled because it occurs in a small extension. The power-law model was used to calculate the reaction rate. The kinetic parameters of the reactions 9, 10, 14, and 15 are presented in Table 3.

Table 3. Kinetic parameters of reactions 9, 10, 14, and 15

Reaction	k_0 / s^{-1}	Ea / (J $kmol^{-1}$)	Reference
9	4.3×10^{13}	5.5471×10^7	20
10	2.38×10^{17}	1.23305×10^8	14
14	2.195×10^{13}	6.74×10^7	19
15	338	7.8994×10^7	21

k_0: pre-exponential factor; Ea: activation energy.

The equilibrium constant (K_{eq}) of the reactions 7, 8, and 10 is calculated according to equation 16. All coefficients are shown in Table 4.

$$\ln(K_{eq}) = A + \frac{B}{T} + C \ln(T) \quad (16)$$

where A, B and C are the parameters of the equilibrium constant used in Aspen Plus.

Table 4. Equilibrium constant parameters of reactions 7, 8, and 11

Reaction	A	B	C	Reference
7	132.899	−13445.9	−22.4773	22-24
8	216.049	−12431.7	−35.4819	22-24
11	177.6	−10266.5	−28.9	18

A, B and C: the parameters of the equilibrium constant used in Aspen Plus.

Rate-base model

The RateFrac routine is used to simulate the absorption and stripper columns. This routine uses the rate-based model for mass and energy balance calculations in columns where there is no thermodynamic equilibrium in the stages.[25] To correct deviations from equilibrium, the rate-based model considers the influence of chemical reactions on mass and energy transfer rates, based on Maxwell-Stefan equations[3] and the Two-Film Theory.[4] The reactions take place in the liquid phase, which should be discretized to increase the model's accuracy, as shown in Figure 3. The film is discretized into 5 sections. According to the results of Schneider *et al.*,[26-28] this value results in errors around 10^{-5} in the composition profiles of the main species.

Discretization also needs to be performed heterogeneously because sections closer to the interface offer less resistance to mass transfer, while sections closer to the bulk solution offer greater resistance. This can be done through the film discretization ratio, which determines the ratio between the thickness of adjacent sections. In this work, the discretization ratio of the liquid film is 5: the section adjacent to the interface is five times smaller than the section adjacent to it and, subsequently to the last section in the direction of the bulk solution. The vapor phase does not require discretization, as no reactions occur in this phase.

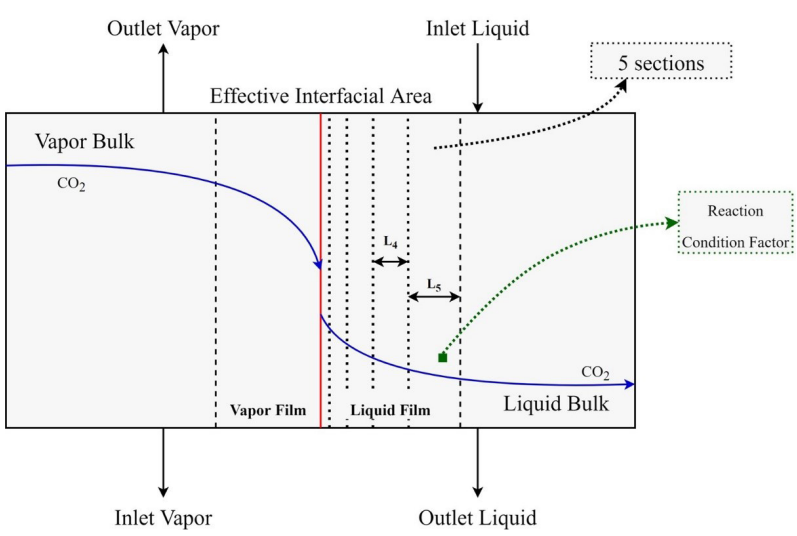

Figure 3. Visual scheme of two-film theory applied to this work.

Another important parameter for the rate-based model is the reaction condition factor, which is illustrated by the green point in Figure 3. This parameter determines the location, in each section of the discretized film, where reaction rates will be calculated. This factor works as a weight between the conditions at the interface and at the bulk solution, through equation 17.

$$C_{avg} = \text{Factor}*C_{bulk} + (1 - \text{Factor})*C_{interface} \quad (17)$$

where C represents variables such as concentration and temperature. Factors close to 1 indicate a greater influence of the conditions within the solution, while factors close to 0 indicate a greater influence of the interface's conditions. The reaction condition factor adopted in this work is 0.9, indicating a greater influence of the conditions within the solution.

Mass transfer and hydraulic correlations

One of the most important steps of the development of a representative model is the choice of correct correlations to calculate the parameters of the rate-based model: mass transfer coefficients, interfacial area, and liquid holdup. Wrong choices of these correlations imply in inaccurate calculations of the mass transfer inside the column. Ultimately, these errors result in wrong estimations of composition and energy consumption.

Aspen Plus provides several correlations to calculate the rate-based parameters. In general, the choice of correct correlations is a function of column diameter, operational conditions, liquid and vapor transport properties, the type and geometry of packing used in the column. The evaluated correlations to calculate liquid holdup, interfacial area and mass transfer coefficients are shown in Tables 5, 6 and 7, respectively.

Correlation calculations require knowledge of several thermodynamic and transport properties. The main equations used to calculate these properties are presented in Table 8 and are widely available in the literature.

An exhausted try and error procedure could be used to find the best set of correlations that represents the HPC process in a suitable manner. A computational methodology was developed to reduce the user's effort. The following procedure tests all the possible combinations (of correlations) that better model the process, in an automatic way. Data from Figure 2 is compared against the model results to validate the best set of correlations.

The conventional way to evaluate the influence of parameters in a mathematical model is through sensitivity analysis. However, Aspen Plus[14] does not allow modification of correlations through the built-in tool. A MATLAB[34] script was developed, and the analysis can be performed automatically. It is necessary to create an interface that enables the communication between the two software, through the creation of a Component Object Model (COM). The MATLAB built-in function actxserver is used for the COM creation. Figure 4 presents the flowchart of the developed MATLAB script.

Once the interface between the software is created (highlighted by red lines), the sensitivity analysis determines the combination of correlations to be used. This information is fed to the Aspen Plus simulation through COM. Once the simulation is run, the results are imported into MATLAB via COM and the error is calculated for each used variable to validate the model. The procedure is repeated until every point of the sensitive analysis is evaluated. At the end, the results are saved in a spreadsheet file and the best combination is printed to the user.

Table 5. Correlations evaluated for stage liquid holdup

Absorption column	Stripper column
Stichlmair *et al.*[11]	Stichlmair *et al.*[11]
$h_L = 0.555 Fr_L^{1/3}\left(1+20\Delta P^2\right)*h_p*A_t$	$h_L = 0.555 Fr_L^{1/3}\left(1+20\Delta P^2\right)*h_p*A_t$
Rocha *et al.*[7]	Billet *et al.*[13]
$h_L = \left(\frac{4F_t}{S}\right)^{2/3}\left(\frac{3\mu^L u_s^L}{\rho_t^L g_{eff}\sin\theta}\right)^{1/3}*h_p*A_t$	$h_L = \left(\frac{12\mu^L a_p^2 u_s^L}{\rho_t^L g}\right)^{1/3}*h_p*A_t$
Billet *et al.*[13]	
$h_L = \left(\frac{12\mu^L a_p^2 u_s^L}{\rho_t^L g}\right)^{1/3}*h_p*A_t$	

h_L / m^3: liquid holdup; h_p / m: packing section height; A_t / m^2: column cross-sectional area; Fr_L: Froude number for the liquid; ΔP / Pa: pressure drop; S / m: slant height of a corrugation; μ^L / (Pa s): liquid viscosity; u_s^L / (m s^{-1}): superficial velocity for the liquid; ρ_t^L / (kg m^{-3}): liquid density; g / (m s^{-2}): gravity; g_{eff} / (m s^{-2}): effective gravity; θ / degree: angle with horizontal of falling film or corrugation channel; a_p / (m^2 m^{-3}): specific packing.

Table 6. Correlations evaluated for interfacial area

Absorption column	Stripper column
Billet *et al.*[13]	Onda *et al.*[10]
$a^I = \frac{1.5}{\sqrt{a_p d_h}}\left(\frac{u_s^L d_h \rho_t^L}{\mu^L}\right)^{-0.2}\left(\frac{\left(u_s^L\right)^2 d_h \rho_t^L}{\sigma}\right)^{0.75}\left(\frac{\left(u_s^L\right)^2}{g d_h}\right)^{-0.45} * a_p * h_p * A_t$	$a^I = \left[1-\exp\left(-1.45\left(\frac{\sigma_c}{\sigma}\right)^{0.75} Re_L^{0.1} Fr_L^{-0.05} We_L^{0.2}\right)\right] * a_p * h_p * A_t$
Rocha *et al.*[7]	Billet *et al.*[13]
$a^I = \frac{29.12\left(We_L Fr_L\right)^{0.15} S^{0.359}}{Re_L^{0.2}\varepsilon^{0.6}\left(\sin\theta\right)^{0.3}\left(1-0.93\cos\gamma\right)} * a_p * F_{se} * h_p * A_t$	$a^I = \frac{1.5}{\sqrt{a_p d_h}}\left(\frac{u_s^L d_h \rho_t^L}{\mu^L}\right)^{-0.2}\left(\frac{\left(u_s^L\right)^2 d_h \rho_t^L}{\sigma}\right)^{0.75}\left(\frac{\left(u_s^L\right)^2}{g d_h}\right)^{-0.45} * a_p * h_p * A_t$
Bravo *et al.*[29]	Bravo *et al.*[29]
$a^I = a_p * h_p * A_t$	$a^I = 19.78 a_p \left(Ca_L Re_V\right)^{0.392} * \frac{\sigma^{0.5}}{h_p^{0.4}} * A_t * h_p$
Tsai *et al.*[30]	Tsai *et al.*[30]
$a^I = 1.34\left[\left(We_L\right)\left(Fr_L\right)^{-1/3}\right]^{0.116}$	$a^I = 1.34\left[\left(We_L\right)\left(Fr_L\right)^{-1/3}\right]^{0.116}$

a^I / m^2: total interfacial area; d_h / m: hydraulic diameter; ρ_t^L / (kg m^{-3}): liquid density; u_s^L / (m s^{-1}): superficial velocity for the liquid; μ^L / (Pa s): liquid viscosity; σ / (N m^{-1}): surface tension of the liquid; σ_c / (N m^{-1}): critical surface tension of the packaging; a_p / (m^2 m^{-3}): specific packing; g / (m s^{-2}): gravity; h_p / m: packing section height; A_t / m^2: column cross-sectional area; Fr_L: Froude number for the liquid; We_L: Weber's number for the liquid; S / m: Slant height of a corrugation; Re_L: Reynolds number for the liquid; Re_V: Reynolds number for the vapor; ε: void fraction of the packing; θ / degree: angle with horizontal of falling film or corrugation channel; γ / degree: contact angle between solid and liquid film; F_{se}: factor for surface enhancement; A_t / m^2: column cross-sectional area; u_s^L / (m s^{-1}): superficial velocity for the liquid; Ca_L: capilar number.

Table 7. Correlations evaluated for mass transfer coefficients

Absorption column	Stripper column
Rocha *et al.*[7]	Onda *et al.*[10]
$k_{i,k}^L = 2\sqrt{\frac{D_{i,k}^L u_{Le}}{\pi S C_E}}$	$k_{i,k}^L = 0.0051\left(Re_L'\right)^{0.667} Sc_{L,i,k}^{-0.5}\left(a_p d_p\right)^{0.4}\left(\frac{\mu^L g}{\rho_t^L}\right)^{0.333}$
$k_{i,k}^V = 0.054\frac{D_{i,k}^V}{S} Re_V^{0.8} Sc_{V,i,k}^{0.333}$	$k_{i,k}^V = 2 Re_V^{0.7} Sc_{V,i,k}^{0.333} a_p D_{i,k}^V \left(a_p d_p\right)^{-2}$ for dp < 0.015 m
	$k_{i,k}^V = 5.23 Re_V^{0.7} Sc_{V,i,k}^{0.333} a_p D_{i,k}^V \left(a_p d_p\right)^{-2}$ for dp > 0.015 m
Bravo *et al.*[29]	Bravo *et al.*[29]
$k_{i,k}^L = 2\sqrt{\frac{D_{i,k}^L}{\pi t_L}}$	$k_{i,k}^L = 0.0051\left(Re_L'\right)^{0.667} Sc_{L,i,k}^{-0.5}\left(a_p d_p\right)^{0.4}\left(\frac{\mu^L g}{\rho_t^L}\right)^{0.333}$
$k_{i,k}^V = 0.0338\frac{D_{i,k}^V}{d_{eq}} Re_V^{0.8} Sc_{V,i,k}^{0.333}$	$k_{i,k}^V = 2 Re_V^{0.7} Sc_{V,i,k}^{0.333} a_p D_{i,k}^V \left(a_p d_p\right)^{-2}$ for dp < 0.015 m
	$k_{i,k}^V = 5.23 Re_V^{0.7} Sc_{V,i,k}^{0.333} a_p D_{i,k}^V \left(a_p d_p\right)^{-2}$ for dp > 0.015 m

$k^L_{i,k}$ / (m s^{-1}): binary mass transfer coefficient to liquid; $k^V_{i,k}$ / (m s^{-1}): binary mass transfer coefficient for vapor; $D^V_{i,k}$ / (m s^{-2}): vapor diffusivity; $D^L_{i,k}$ / (m s^{-2}): liquid diffusivity; S / m: side dimension a corrugation; C_E: correction factor for surface renewal; u_{Le} / (m s^{-1}): effective velocity through the channel for liquid; Re_V: Reynolds number for the vapor; $Sc_{V,i,k}$: Schmidt number for the vapor; $Sc_{L,i,k}$: Schmidt number for the liquid; t_L / s: residence time for the liquid; d_{eq} / m: equivalent diameter; Re'_L: Reynolds number for the liquid based on the wet surface; a_p / (m^2 m^{-3}): specific packing; d_p / m: nominal packing size; μ^L / (Pa s): liquid viscosity; g / (m s^{-2}): gravity; ρ_t^L / (kg m^{-3}): liquid density.

Table 8. Correlations used for thermodynamic and transport properties calculation

Property	Correlation
Pressure drop in the column	Wallis/Aspen[31]
Heat transfer coefficient	Chilton and Colburn[32]
Flow model	mixed
Density	Rackett, DIPPR[32,33]
Viscosity	DIPPR[33]
Superficial tension	DIPPR[33]
Binary diffusivity	Nernst-Hartley[33]
Thermal conductivity	DIPPR and NIST ThermoM[33]

DIPPR: Design Institute for Physical Property Research.

Results and Discussion

The correlations presented in Tables 5 to 7 were evaluated in the Aspen Plus regarding their ability to represent the HPC process. By using the procedure mentioned in the experimental description, 384 combinations were analyzed. For didactic purposes, 12 combinations were selected for discussion, as shown in Table 9.

Figure 5 presents the errors of variables in the absorption column: CO_2 composition in clean gas, top and bottom temperatures. The combinations 2 to 8 obtained

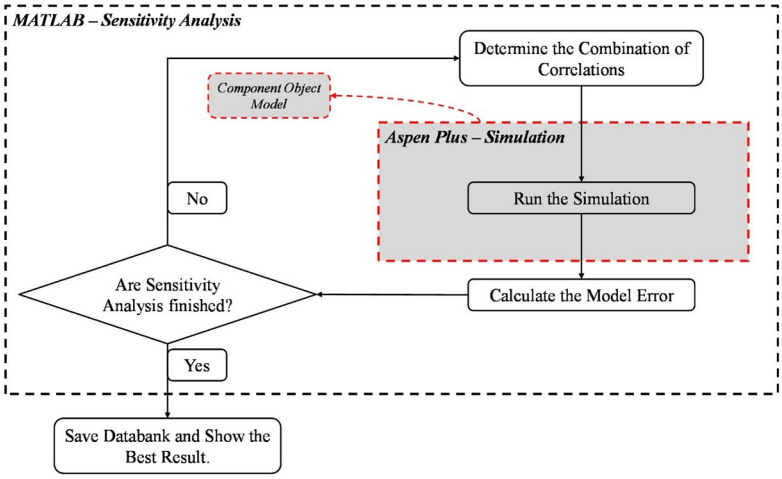

Figure 4. Communication between MATLAB and Aspen Plus software implemented to evaluate the studied correlations.

Table 9. Combinations of correlations selected

Combination	ABS column			STP column		
	Mass transfer coefficient	Interfacial area	Liquid holdup	Mass transfer coefficient	Interfacial area	Liquid holdup
1	Rocha *et al.*[7]	Rocha *et al.*[7]	Stichlmair *et al.*[11]	Onda *et al.*[10]	Tsai *et al.*[30]	Stichlmair *et al.*[11]
2	Rocha *et al.*[7]	Rocha *et al.*[7]	Stichlmair *et al.*[11]	Bravo *et al.*[29]	Onda *et al.*[10]	Stichlmair *et al.*[11]
3	Rocha *et al.*[7]	Rocha *et al.*[7]	Stichlmair *et al.*[11]	Bravo *et al.*[29]	Bravo *et al.*[29]	Stichlmair *et al.*[11]
4	Rocha *et al.*[7]	Rocha *et al.*[7]	Stichlmair *et al.*[11]	Bravo *et al.*[29]	Billet *et al.*[13]	Stichlmair *et al.*[11]
5	Rocha *et al.*[7]	Rocha *et al.*[7]	Stichlmair *et al.*[11]	Bravo *et al.*[29]	Tsai *et al.*[30]	Stichlmair *et al.*[11]
6	Rocha *et al.*[7]	Rocha *et al.*[7]	Stichlmair *et al.*[11]	Bravo *et al.*[29]	Tsai *et al.*[30]	Billet *et al.*[13]
7	Rocha *et al.*[7]	Rocha *et al.*[7]	Bravo *et al.*[35]	Bravo *et al.*[29]	Tsai *et al.*[30]	Stichlmair *et al.*[11]
8	Rocha *et al.*[7]	Rocha *et al.*[7]	Billet *et al.*[13]	Bravo *et al.*[29]	Tsai *et al.*[30]	Stichlmair *et al.*[11]
9	Rocha *et al.*[7]	Bravo *et al.*[35]	Stichlmair *et al.*[11]	Bravo *et al.*[29]	Tsai *et al.*[30]	Stichlmair *et al.*[11]
10	Rocha *et al.*[7]	Billet *et al.*[13]	Stichlmair *et al.*[11]	Bravo *et al.*[29]	Tsai *et al.*[30]	Stichlmair *et al.*[11]
11	Rocha *et al.*[7]	Tsai *et al.*[30]	Stichlmair *et al.*[11]	Bravo *et al.*[29]	Tsai *et al.*[30]	Stichlmair *et al.*[11]
12	Bravo *et al.*[35]	Rocha *et al.*[7]	Stichlmair *et al.*[11]	Bravo *et al.*[29]	Tsai *et al.*[30]	Stichlmair *et al.*[11]

ABS: absorber; STP: stripper.

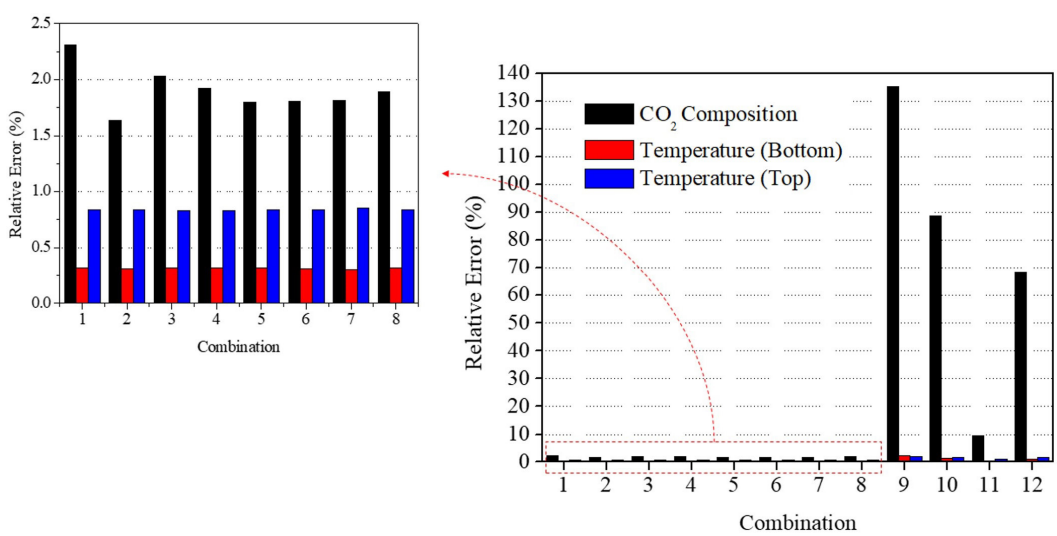

Figure 5. Relative error of main variables in the absorber column.

the best results with errors below 2.5%, considering all the variables. The choice of combinations does not significantly impact the prediction of top and bottom temperatures.

Figure 6 presents the errors of variables in the stripper column: reboiler steam consumption, top and bottom temperatures. Considering the steam consumption, the best results were obtained with combinations 3, 5, and 6. The prediction of top and bottom temperatures was not significantly affected by the combination of correlations.

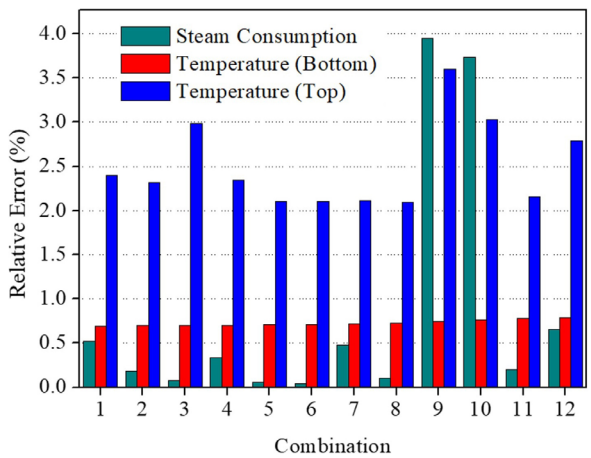

Figure 6. Relative error of the main variables in the stripper column.

A more detailed discussion is presented in the next paragraphs. Table 10 shows the average CO_2/K_2CO_3 binary mass transfer coefficient in the absorption column for all combinations.

Table 10. Average mass transfer coefficients in the absorption column

Combination	CO_2/K_2CO_3 overall mass transfer coefficient / (kmol h^{-1})
1-11 (Rocha *et al.*[7])	13855.35
12 (Bravo *et al.*[35])	3715.10

Considering the combinations 5 and 12, the difference between then is the correlation used to calculate the mass transfer coefficient in the absorption column: combination 5 uses Bravo *et al.*[7] and 12 uses Bravo *et al.*[35] The choice by one or other has a strong impact in the prediction of CO_2 composition in the clean gas. In the first case, the relative error is 1.8% while in the last case, this error is 68.6%. The Bravo *et al.*[35] correlation is based on packing corrugation side dimension and the effective velocity. The Rocha *et al.*[7] considers the liquid residence time but not the effective velocity. The considerations adopted by Rocha *et al.*[7] correlation results in an increase in the mass transfer coefficient and lower errors. In this way, Rocha *et al.*[7] is the most suitable correlation to calculate the mass transfer coefficient in the absorption column.

Considering the combinations 5, 9, 10, and 11, the difference between then is the used correlation to calculate the interfacial area in the absorption column, as shown in Table 11. According to Hemmati *et al.*,[12] this parameter mainly depends on gas flow rate and density. Liquid flow rate is proportional to effective area: greater liquid velocities results in a higher packing wettability. Therefore, the effective interfacial area is increased, resulting in a higher mass transfer.

Table 11. Average effective interfacial area in the absorption column

Combination	Interfacial area / m^2
1-8 and 12 (Rocha *et al.*[7])	166.7342
9 (Bravo *et al.*[35])	36.1409
10 (Billet *et al.*[13])	59.6639
11 (Tsai *et al.*[30])	149.2431

The combination 9 showed the highest error for the absorption column. This can be attributed to the high number of used variables in correlations Bravo *et al.*[35] Moreover, the interfacial area calculated by this equation is affected by parameters that has a strong dependence of gas and liquid flow rates, as Reynolds number. The absorption column operates in a turbulent regime, which is characterized by a high surface velocity and a high Reynolds number (Re > 10.000).[33,36] According to the Bravo *et al.*[35] correlation, the value of the interfacial area is inversely proportional to the Reynolds number, the higher the Reynolds number the lower the value of the interfacial area.

Considering the absorption column, the combinations 7 and 8 shows that the choice of correlation used to calculate liquid holdup does not significantly impact the model, as can be seen in Figure 5. In addition, Table 12 does not show any modification in the value of calculated liquid holdup.

Table 12. Average stage liquid holdup in the absorption column

Combination	Liquid holdup / m^3
1-6 and 9-12 (Stichlmair *et al.*[11])	102.19
7 (Bravo *et al.*[35])	102.19
8 (Billet *et al.*[13])	102.19

Examining the stripper column, as mentioned before, the lowest errors were obtained for combinations 3, 5 and 6, while the highest errors were combinations 9 and 10. However, combination 5 and 9 use the same set of correlations. How can they result in opposite outcomes?

It suggests that correlations do not have any impact on the stripper column. The errors of the stripper are much more correlated to the errors of absorption column: the highest errors of absorber are for combinations 9, 10, 11 and 12; these errors are impact the stripper, resulting in wrong predictions of it. Dutta *et al.*[37] states that the stripper column operates close to the equilibrium conditions and can be modeled with equilibrium model. This explains why the correlations do not directly impact the desorption process.

Other operating conditions

With the definition of the best combination of correlations, the model was used to predict the process behavior under two different operational conditions: operation with catalyst at the beginning of the campaign (characterized by the lower production of CO_2 in the reactor); and operation with catalyst at the end of the campaign (characterized by the higher production of CO_2 in the reactor). Table 13 presents the results using combination 5 for the used correlations. Even with very different conditions, acceptable errors were obtained.

Table 13. Results for different operating conditions

Validation variables	Relative error for the case of low CO_2 production in the reactor / %	Relative error for the case of high CO_2 production in the reactor / %
CO_2 composition	6.32	1.91
Temperature bottom (ABS)	1.68	1.02
Temperature top (ABS)	1.85	2.49
Steam consumption	1.03	0.68
Temperature bottom (STP)	5.06	1.58
Temperature top (STP)	4.02	2.43

ABS: absorber; STP: stripper.

Conclusions

In the present work, different combinations of correlations for calculating mass transfer coefficient, interfacial area and liquid holdup were evaluated and compared to estimate key parameters of an HPC process promoted with H_3BO_3. The best set of correlations is Bravo *et al.*[29] to calculate the mass transfer coefficients and interfacial area in the absorber; Stichlmair *et al.*[11] to calculate the liquid holdup in the absorber column. The stripper column was not affected by the correlation and can be modeled using equilibrium thermodynamic consideration. This work developed an automatic procedure to evaluate a high number of correlations, reducing time and effort during the process evaluation. Lastly, the industrial plant data used to validate the model is valuable for academic purposes.

Acknowledgments

The authors thank the National Council for Scientific and Technological Development (CNPq) for the financial support.

References

1. Smith, K. H.; Nicholas, N. J.; Stevens, G. W.; *Absorption-Based Post-Combustion Capture of Carbon Dioxide*; Feron, P. H. M., ed.; Woodhead: Cambidge, 2016, p. 145. [Crossref]
2. Ayittey, F. K.; Saptoro, A.; Kumar, P.; Wong, M. K.; *IOP Conf. Ser.: Mater. Sci. Eng.* **2020**, *778*, 012082. [Crossref]
3. Maxwell, J. C.; *Philos. Trans. R. Soc. London* **1867**, *157*, 49. [Crossref]
4. Whitman, W. G.; *Int. J. Heat Mass Transfer* **1962**, *5*, 429. [Crossref]
5. Gaspar, J.; Cormos, A.-M.; *Int. J. Greenhouse Gas Control* **2012**, *8*, 45. [Crossref]
6. Wang, G. Q.; Yuan, X. G.; Yu, K. T.; *Chem. Eng. Process.: Process Intensif.* **2006**, *45*, 691. [Crossref]
7. Rocha, J. A.; Bravo, J. L.; Fair, J. R.; *Ind. Eng. Chem. Res.* **1996**, *35*, 1660. [Crossref]
8. Zhang, Y.; Chen, C.-C.; *Energy Procedia* **2013**, *37*, 1584. [Crossref]
9. Qi, G.; Wang, S.; Yu, H.; Wardhaugh, L.; Feron, P.; Chen, C.; *Int. J. Greenhouse Gas Control* **2013**, *17*, 450. [Crossref]
10. Onda, K.; Takeuchi, H.; Okumoto, Y.; *J. Chem. Eng. Jpn.* **1968**, *1*, 56. [Crossref]
11. Stichlmair, J.; Bravo, J. L.; Fair, J. R.; *Gas Sep. Purif.* **1989**, *3*, 19. [Crossref]
12. Hemmati, A.; Farahzad, R.; Surendar, A.; Aminahmadi, B.; *Process Saf. Environ. Prot.* **2019**, *126*, 214. [Crossref]
13. Billet, R.; Schultes, M.; *Chem. Eng. Technol.* **1993**, *16*, 1. [Crossref]
14. *Aspen Plus*, v.10; Aspen Technology, Massachusetts Institute of Technology, USA, 2010.
15. Khalfe, N. M.; Lahiri, S. K.; Sawke, S. K.; *Chem. Ind. Chem. Eng. Q.* **2011**, *17*, 17. [Crossref]
16. Conway, R. A.; Waggy, G.T.; Spiegel, M. H.; Berglund, R. L.; *Environ. Sci. Technol.* **1983**, *17*, 107. [Crossref]
17. Ahmadi, M.; Gomes, V. G.; Ngian, K.; *Sep. Purif. Technol.* **2008**, *63*, 107. [Crossref]
18. Smith, K. H.; Anderson, C. J.; Tao, W.; Endo, K.; Mumford, K. A.; Kentish, S. E.; Qader, A.; Hooper, B.; Stevens, G. W.; *Int. J. Greenhouse Gas Control* **2012**, *10*, 64. [Crossref]
19. Guo, D.; Thee, H.; da Silva, G.; Chen, J.; Fei, W.; Kentish, S.; Stevens, G. W.; *Environ. Sci. Technol.* **2011**, *45*, 4802. [Crossref]

20. Pinsent, B. R. W.; Pearson, L.; Roughton, F. J. W.; *Trans. Faraday Soc.* **1956**, *52*, 1512. [Crossref]
21. An, W.; Lin, Z.; Chen, J.; Zhu, J.; *Ind. Eng. Chem. Res.* **2014**, *53*, 6056. [Crossref]
22. Jou, F.-Y.; Mather, A. E.; Otto', F. D.; *Ind. Eng. Chem. Process Des. Dev* **1982**, *21*, 539. [Crossref]
23. Jou, F. Y.; Carroll, J. J.; Mather, A. E.; Otto, F. D.; *J. Chem. Eng. Data* **1993**, *38*, 75. [Crossref]
24. Jou, F. -Y; Carroll, J. J.; Mather, A. E.; Otto, F. D.; *Can. J. Chem. Eng.* **1993**, *71*, 264. [Crossref]
25. Léonard, G.: *Optimal Design of a CO2 Capture Unit with Assessment of Solvent Degradation*, PhD Thesis, University of Liege, 2013. [Link] accessed in September 2022
26. Schneider, R.; Sander, F.; Górak, A.; *Chem. Eng. Process.: Process Intensif.* **2003**, *42*, 955. [Crossref]
27. Kenig, E. Y.; Schneider, R.; Górak, A.; *Chem. Eng. Sci.* **2001**, *56*, 343. [Crossref]
28. Mayer, J.; Schneider, R.; Kenig, E.; Górak, A.; Wozny, G.; *Comput. Chem. Eng.* **1999**, *23*, S843. [Crossref]
29. Bravo, J. L.; Fair, J. R.; *Ind. Eng. Chem. Process Des. Dev.* **1982**, *21*, 162. [Crossref]
30. Tsai, R. E.; Seibert, A. F.; Eldridge, R. B.; Rochelle, G. T.; *AIChE J.* **2011**, *57*, 1173. [Crossref]
31. Suess, P.; Spiegel, L.; *Chem. Eng. Process.* **1992**, *31*, 119. [Crossref]
32. Stewart, W. E.; *AIChE J.* **1993**, *41*, 202. [Crossref]
33. Poling, B. E.; Prausnitz, J. M.; *The Properties of Gases and Liquids*, vol. 1, 5th ed.; Elsevier: London, UK, 2011.
34. *MATLAB*, v.R2018b; MathWorks, Stanford University, USA, 2018.
35. Bravo, J. L.; Rocha, J. R.; Fair, J. R.; *Inst. Chem. Eng. Symp. Ser.* **1992**, *1*, A489. [Link] accessed in September 2022
36. Li, W.; Yu, K.; Yuan, X.; Liu, B.; *Int. J. Heat Mass Transfer* **2015**, *88*, 775. [Crossref]
37. Dutta, R.; Nord, L. O.; Bolland, O.; *Fuel* **2017**, *202*, 85. [Crossref]

Submitted: May 16, 2022
Published online: September 21, 2022

This is an open-access article distributed under the terms of the Creative Commons Attribution License.